

Article

Direct One-Step Growth of Bimetallic Ni₂Mo₃N on Ni Foam as an Efficient Oxygen Evolution Electrocatalyst

Sang Heon Park ¹, Soon Hyung Kang ^{2,*} and Duck Hyun Youn ^{1,*} 

¹ Department of Chemical Engineering, Interdisciplinary Program in Advanced Functional Materials and Devices Development, Kangwon National University, Chuncheon 24341, Korea; parksh31@kangwon.ac.kr

² Department of Chemistry Education, Chonnam National University, Gwangju 61186, Korea

* Correspondence: skang@jnu.ac.kr (S.H.K.); youndh@kangwon.ac.kr (D.H.Y.)

Abstract: A simple and economical synthetic route for direct one-step growth of bimetallic Ni₂Mo₃N nanoparticles on Ni foam substrate (Ni₂Mo₃N/NF) and its catalytic performance during an oxygen evolution reaction (OER) are reported. The Ni₂Mo₃N/NF catalyst was obtained by annealing a mixture of a Mo precursor, Ni foam, and urea at 600 °C under N₂ flow using one-pot synthesis. Moreover, the Ni₂Mo₃N/NF exhibited high OER activity with low overpotential values (336.38 mV at 50 mA cm⁻² and 392.49 mV at 100 mA cm⁻²) and good stability for 5 h in Fe-purified alkaline electrolyte. The Ni₂Mo₃N nanoparticle surfaces converted into amorphous surface oxide species during the OER, which might be attributed to the OER activity.

Keywords: water splitting; oxygen evolution reaction; bimetallic nitride; Ni₂Mo₃N; Ni foam



Citation: Park, S.H.; Kang, S.H.; Youn, D.H. Direct One-Step Growth of Bimetallic Ni₂Mo₃N on Ni Foam as an Efficient Oxygen Evolution Electrocatalyst. *Materials* **2021**, *14*, 4768. <https://doi.org/10.3390/ma14164768>

Academic Editor: Ivano E. Castelli

Received: 28 June 2021

Accepted: 19 August 2021

Published: 23 August 2021

Publisher's Note: MDPI stays neutral with regard to jurisdictional claims in published maps and institutional affiliations.



Copyright: © 2021 by the authors. Licensee MDPI, Basel, Switzerland. This article is an open access article distributed under the terms and conditions of the Creative Commons Attribution (CC BY) license (<https://creativecommons.org/licenses/by/4.0/>).

1. Introduction

Hydrogen (H₂) is a promising energy carrier due to its high mass-specific energy density (142 MJ kg⁻¹), high utilization efficiency, and zero carbon emission when generated from renewable energy sources. Electrochemical water splitting from renewables such as solar or wind energy is considered a clean and efficient route for hydrogen production [1–4]. Water splitting consists of hydrogen evolution reaction (HER) and oxygen evolution reaction (OER). The four electrons involved in OER (4OH⁻ → 2H₂O + O₂ + 4e⁻) are kinetically sluggish relative to the two electrons involved in HER, requiring large overpotential values [5–9]. Ir- and Ru-based materials are typical catalysts for OER, but their high cost and scarcity restrict their widespread application [10–12]. Thus, developing alternative OER electrocatalysts based on low-cost and abundant materials is urgent for the large-scale proliferation of water-splitting systems.

Materials that include transition metals, such as transition metal oxides, transition metal nitrides (TMNs), and transition metal oxynitrides, demonstrated very promising OER activity [13,14]. Among them, various monometallic TMNs including Ni₃N, Co₄N, HfN, and Mn₃N₂ have been investigated as low-cost electrocatalysts [15–18]. TMNs possessing physical hardness, chemical stability, electrical conductivity, and unique electronic structure have been traditionally used as catalysts for chemical processes [19,20], and recently showed potential for energy applications [21,22]. However, these monometallic TMNs still exhibit limited OER performance. Designing bimetallic TMNs has proven to be an effective way to improve the OER performance of monometallic TMNs, which is expected to show the synergy between two distinct metal species [23,24]. In bimetallic TMNs, the presence of a second metal atom supplied more active sites and enhanced electronic conductivity, achieving higher OER activity compared to monometallic catalysts [25,26]. Among the various bimetallic TMNs, Ni-Mo nitrides have been extensively explored as OER electrocatalysts due to their high activity and stability. Although progress has been made, Ni-Mo nitrides are traditionally prepared by a complex method involving a two- or multistep annealing process. This typically involves hydrothermal Ni-Mo oxide formation

and subsequent nitridation using NH_3 gas for Ni-Mo nitride formation, making synthesis a challenge [27–31].

In this work, we report a simple and economical synthetic route for direct one-step growth of bimetallic $\text{Ni}_2\text{Mo}_3\text{N}$ nanoparticles on Ni foam substrate ($\text{Ni}_2\text{Mo}_3\text{N}/\text{NF}$) for use as an OER catalyst. The $\text{Ni}_2\text{Mo}_3\text{N}/\text{NF}$ catalyst was prepared by annealing Mo precursor, Ni foam, and urea at $600\text{ }^\circ\text{C}$ under N_2 flow in one pot. During annealing, inert N_2 gas was used in exchange for toxic ammonia gas. In addition, no Ni precursor was added because Ni foam acted as the Ni source. Therefore, the suggested fabrication method is simple, economical, and eco-friendly. The resultant $\text{Ni}_2\text{Mo}_3\text{N}/\text{NF}$ catalyst exhibited impressive OER catalytic performance with small overpotential values of 336.38 and 392.49 mV at current densities of 50 and 100 mA cm^{-2} , respectively, and excellent stability over 5 h of operation at 50 mA cm^{-2} . The high activity and stability with this simple synthetic method suggest that our $\text{Ni}_2\text{Mo}_3\text{N}/\text{NF}$ catalyst could be a promising electrocatalyst for OER.

2. Materials and Methods

2.1. Materials

Molybdenum chloride (MoCl_5) was purchased from Alfa Aesar. Urea ($\text{CH}_4\text{N}_2\text{O}$), ethanol ($\text{C}_2\text{H}_5\text{OH}$), and a 1.0 M potassium hydroxide (KOH) solution were purchased from Samchun. Notably, an Fe-free 1.0 M KOH electrolyte was prepared by following a previously reported method to avoid incidental Fe incorporation and consequent OER activity enhancement during the electrochemical tests [32]. For preparation of an Fe-free 1.0 M KOH solution, $\text{Ni}(\text{NO}_3)_2 \cdot 6\text{H}_2\text{O}$ was dissolved in ultrapure water and 1.0 M KOH was added to precipitate high-purity $\text{Ni}(\text{OH})_2$. After three centrifugation and washing cycles, the high-purity $\text{Ni}(\text{OH})_2$ solid was mechanically stirred in 1.0 M KOH for at least 10 min and rested for 3 h. The mixture was centrifuged, and the purified KOH supernatant was transferred to a clean bottle and used as an Fe-free electrolyte. The Ni foam was purchased from Goodfellow (Ni003852), having a pore size of ca. $450\text{ }\mu\text{m}$ and a strut diameter of ca. $70\text{ }\mu\text{m}$. Commercial IrO_2 catalysts were purchased from Alfa Aesar (A17849).

2.2. Synthesis of $\text{Ni}_2\text{Mo}_3\text{N}/\text{NF}$

A measure of 3.66 mmol MoCl_5 was dissolved in 2.53 mL ethanol, then 5.49 mmol urea (molar ratio of urea/Mo = 1.5) was added to the solution, which was stirred for 1 h until the urea was completely dissolved. The solution was transferred to an alumina boat with pieces of Ni foam and annealed at $600\text{ }^\circ\text{C}$ (ramping at $3.3\text{ }^\circ\text{C min}^{-1}$) for 3 h under flowing N_2 gas (100 sccm) to fabricate the $\text{Ni}_2\text{Mo}_3\text{N}/\text{NF}$ electrocatalyst.

2.3. Characterizations

A scanning electron microscope ((SEM, JEOL JSM-7900F) (Jeol, Peabody, MA, USA)) with an energy dispersive X-ray spectrometer (EDS) and a high-resolution transmission electron microscope ((HRTEM, JEM-2100F, JEOL (Acc. Voltage: 200 kV) (Jeol, Peabody, MA, USA)) were used to reveal detailed structural information. Crystalline structures of the prepared catalysts were investigated by X-ray diffraction (XRD, Miniflex 600, Rigaku, Tokyo, Japan) using $\text{Cu-K}\alpha$ (wavelength = 1.5406 \AA) radiation at 40 kV and 15 mA. Surface chemical states were analyzed using X-ray photoelectron spectroscopy (XPS, Thermo Fisher Scientific, K-Alpha, Waltham, MA, USA) with an X-ray source of $\text{Al-K}\alpha_1$. The recorded binding energies were calibrated using the adventitious carbon C 1s peak at 284.8 eV. In addition, the XPS spectra for Ni 2p and Mo 3d were deconvoluted to have area ratios of 1:2 ($2\text{p}_{1/2}:2\text{p}_{3/2}$) and 2:3 ($3\text{d}_{3/2}:3\text{d}_{5/2}$), respectively.

2.4. Electrochemical Tests

Electrochemical characterizations were carried out in a three-electrode cell system using a potentiostat ((PAR, VersaSTAT 4) (Ametek, Berwyn, PA, USA)) under an O_2 -purged Fe-free 1.0 M KOH solution. The $\text{Ni}_2\text{Mo}_3\text{N}/\text{NF}$ ($1 \times 1\text{ cm}^2$) was directly used as a working electrode. The Ag/AgCl (3 M NaCl) and Pt wire were used as a reference and

counter electrode, respectively. All potentials were converted to the reversible hydrogen electrode (RHE) using the equation ($E_{\text{RHE}} = E_{\text{Ag/AgCl}} + 0.059 \text{ pH} + E^{\circ}_{\text{Ag/AgCl}}$). Linear sweep voltammetry (LSV) polarization curves were obtained using iR compensation at a scan rate of 5 mV s^{-1} . The long-term stability test was carried out using the chronopotentiometric method. Electrochemical impedance spectroscopy (EIS) was performed from 10^5 to 10^{-1} Hz with a modulation amplitude of 20 mV at 400 mV overpotential, and EIS plots were fitted with Z-view software.

3. Results and Discussion

Figure S1 shows digital photographs for the synthetic procedure. MoCl_5 was dissolved in ethanol to form a dark-greenish solution (Figure S1a). At this step, MoCl_5 reacts with ethanol vigorously, generating molybdenum orthoester and releasing HCl gas [33,34]. The addition of urea to the solution yielded a viscous Mo-urea complex (Figure S1b) [35,36]. Ni foams and Mo-urea complex were transferred to an alumina boat and annealed at $600 \text{ }^{\circ}\text{C}$ for 3 h under N_2 flow (Figure S1c,d). Consequently, $\text{Ni}_2\text{Mo}_3\text{N}$ nanoparticles grown directly on nickel foam were fabricated (Figure S1e,f). During the synthetic procedure, nitrogen was supplied from urea; thus, toxic ammonia gas was not employed for nitridation. Even more rewarding was that no Ni precursor was added for $\text{Ni}_2\text{Mo}_3\text{N}$ generation because the Ni foam support acted as a Ni source through thermal diffusion [37–40]. These alterations in the technique enabled our synthetic method to be economical and straightforward.

Before further experiments, the annealing temperatures of $\text{Ni}_2\text{Mo}_3\text{N}/\text{NF}$ samples were optimized. Figure S2 displays the XRD patterns of prepared samples at various annealing temperatures from 550 to $650 \text{ }^{\circ}\text{C}$. A pure crystalline $\text{Ni}_2\text{Mo}_3\text{N}$ phase was obtained only at an annealing temperature of $600 \text{ }^{\circ}\text{C}$. At $650 \text{ }^{\circ}\text{C}$, mixed phases of $\text{Ni}_2\text{Mo}_3\text{N}$ and Mo_2N were detected in XRD patterns, while at $550 \text{ }^{\circ}\text{C}$, an oxide phase was observed with low peak intensities of $\text{Ni}_2\text{Mo}_3\text{N}$. Thus, the annealing temperature of $600 \text{ }^{\circ}\text{C}$ was employed as the optimum temperature condition to form $\text{Ni}_2\text{Mo}_3\text{N}/\text{NF}$.

Figure 1a shows SEM images of $\text{Ni}_2\text{Mo}_3\text{N}/\text{NF}$. A three-dimensional porous structure stems from the pristine Ni foam, and a rough surface originates from the growth of the $\text{Ni}_2\text{Mo}_3\text{N}$ particles on the Ni foam. The elemental mapping image of Ni is consistent with Mo and N, indicating that the $\text{Ni}_2\text{Mo}_3\text{N}$ nanoparticles are uniformly dispersed on the Ni foam substrate. Figure 1b and Figure S3 show the TEM image and the corresponding particle size distribution graph of $\text{Ni}_2\text{Mo}_3\text{N}/\text{NF}$, where $7.2 \pm 1.1 \text{ nm}$ $\text{Ni}_2\text{Mo}_3\text{N}$ nanoparticles are observed without heavy aggregation. The observed lattice fringe of 2.21 \AA in the high-resolution TEM (HRTEM) image (Figure 1c) corresponds to the $\text{Ni}_2\text{Mo}_3\text{N}$ (221) plane.

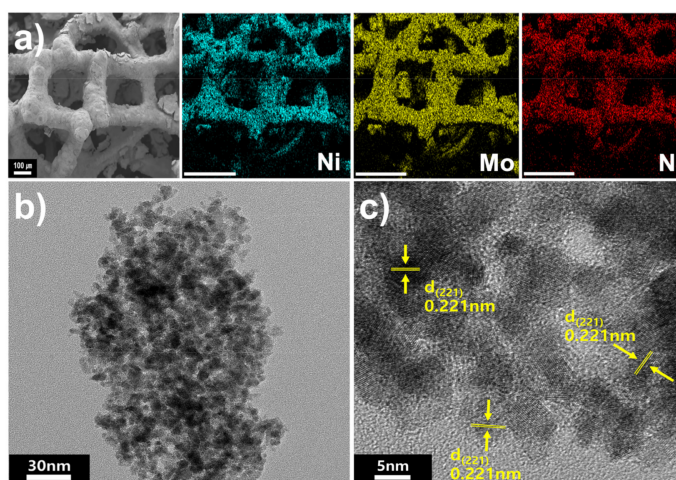


Figure 1. (a) SEM image of $\text{Ni}_2\text{Mo}_3\text{N}/\text{NF}$ and SEM-EDS elemental mapping images (scale bar = 300 μm). (b,c) TEM images of $\text{Ni}_2\text{Mo}_3\text{N}/\text{NF}$.

Figure 2a shows X-ray diffraction (XRD) patterns of Ni₂Mo₃N/NF. The intense peaks at 45, 52, and 76° can be indexed to metallic Ni (JCPDS no. 00-004-0850) from Ni foam. The other diffraction peaks observed at 40.7, 43.1, 45.3, 72.6, and 77.4° correspond to (221), (310), (311), (510), and (520) planes of reference in cubic Ni₂Mo₃N patterns (JCPDS no. 01-089-4564). No other phases such as MoO₃ or Mo₂N were detected; hence, phase-pure Ni₂Mo₃N was grown on the Ni foam. The Ni₂Mo₃N possesses a filled β-manganese structure composed of corner-sharing Mo₆N octahedra and interpenetrated net-like Ni atoms [41,42].

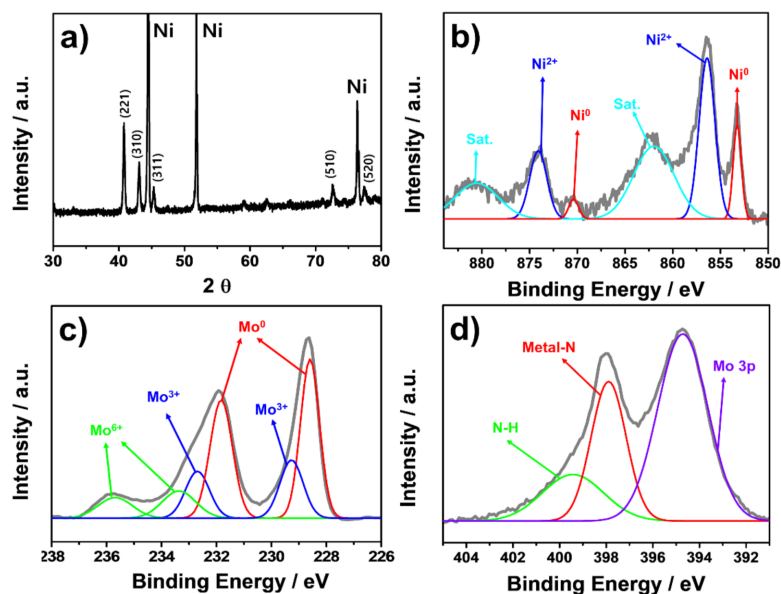


Figure 2. (a) XRD patterns of Ni₂Mo₃N/NF. XPS spectra of Ni₂Mo₃N/NF for (b) Ni 2p, (c) Mo 3d, and (d) N 1s.

The chemical states of Ni₂Mo₃N/NF were analyzed by X-ray photoelectron spectroscopy (XPS). Figure 2b shows the Ni 2p XPS spectra of Ni₂Mo₃N/NF. The peaks shown at 852.9 and 870.4 eV are ascribed to 2p_{3/2} and 2p_{1/2} of metallic Ni (Ni⁰), while the peaks centered at 856.4 and 873.9 eV are due to Ni²⁺ 2p_{3/2} and 2p_{1/2}, respectively [27,33,43,44]. The high-resolution Mo 3d XPS spectra (Figure 2c) can be deconvoluted into three pairs with binding energies of 228.5/231.8, 229.4/232.6, and 233.4/235.7 eV corresponding to Mo⁰, Mo³⁺, and Mo⁶⁺, respectively [33,43,45]. The Mo⁰ and Mo³⁺ valence states originated from Ni₂Mo₃N, and the presence of Mo⁶⁺ is due to surface oxide formation [44–47]. In the N 1s XPS spectra (Figure 2d), the two deconvoluted peaks at 397.9 and 399.5 eV are attributed to metal-N and N-H groups, respectively. The N-H groups are likely associated with surface-adsorbed NH_x species due to reaction with moisture from air exposure [48]. In addition, the peak at 394.7 eV originated from partially overlapped Mo 3p [27,30,31].

Figure 3a exhibits the polarization curves for the OER with Ni₂Mo₃N/NF in an Fe-free 1.0 M KOH solution along with commercial IrO₂ and pure Ni foam for comparison. The observed peak around 1.4 V for Ni₂Mo₃N/NF is ascribed to the oxidation of Ni(II)/Ni(III) or IV [49,50]. The Ni₂Mo₃N/NF exhibited a much higher current density over the whole potential region than the others. The overpotential values of Ni₂Mo₃N/NF at 50 mA cm⁻² and 100 mA cm⁻² were 336.38 mV (η₅₀) and 392.49 mV (η₁₀₀), respectively. The η₅₀ value of Ni₂Mo₃N/NF was even smaller than 450.55 mV for commercial IrO₂. The pure Ni foam did not reach 50 mA cm⁻² in the measured potential range (Figure 3b) and showed poor OER activity with an η₁₀ value of 358.91 mV, suggesting that the loaded Ni₂Mo₃N phase was mainly responsible for the OER activity. In addition, at an overpotential value of 400 mV, the current density of the Ni₂Mo₃N/NF reached 111.18 mA cm⁻², which is 4.5 and 21.6 times higher than commercial IrO₂ and Ni foam, respectively (Figure 3b).

The Ni₂Mo₃N/NF recorded one of the best OER catalytic performances among reported TMN-based electrocatalysts (Table S1).

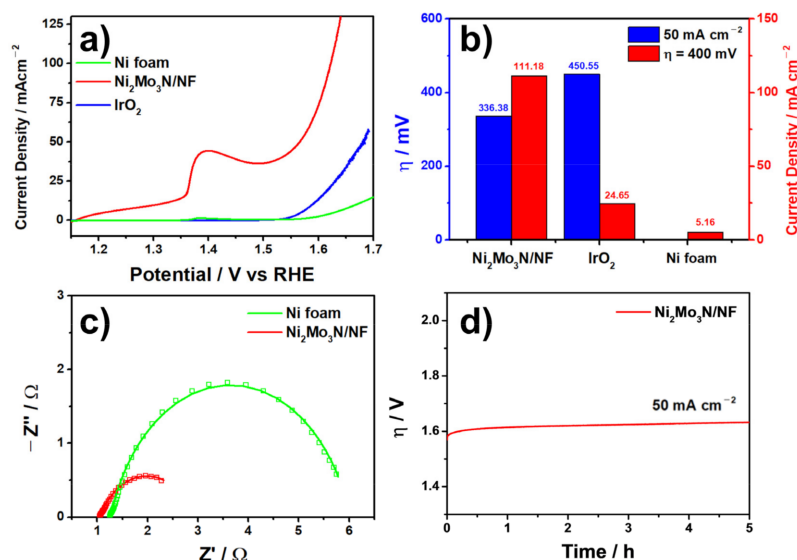


Figure 3. Electrochemical characterization of the prepared catalysts. (a) Polarization curves (1.0 M KOH solution), (b) bar graphs showing overpotentials at 50 mA cm⁻² and current densities at an overpotential of 400 mV, (c) Nyquist plots, and (d) durability measurement.

The electrochemical active surface area (ECSA), the area of the electrode materials that is accessible to the electrolyte for electrochemical reaction, was estimated by the double layer capacitance (C_{dl}) method (Figure S4). The measured C_{dl} value for Ni₂Mo₃N/NF is 347.24 mF cm⁻², whereas pure Ni foam and commercial IrO₂ recorded small C_{dl} values of 0.68 and 0.55 mF cm⁻², respectively. The high ECSA of Ni₂Mo₃N/NF suggests that the enhanced contact area between the catalyst and electrolyte is fruitful for improving the electrochemical activity of Ni₂Mo₃N/NF.

Electrochemical impedance spectroscopy (EIS) was conducted to characterize the prepared catalysts further, and the resulting Nyquist plots are presented in Figure 3c. A semicircle in the Nyquist plot represents the charge transfer resistance (R_{ct}) and corresponding capacitance, describing the charge-transfer process at the catalyst/electrolyte interface. Generally, the R_{ct} value is inversely proportional to electrochemical activity. The Ni₂Mo₃N/NF catalyst exhibited a smaller R_{ct} value (1.861 Ω) than pure Ni foam (4.742 Ω), indicating enhanced OER catalytic activity due to the synergy between the Ni₂Mo₃N phase with high activity and the Ni foam providing a large surface area and high conductivity.

Chronopotentiometry tests were carried out to characterize the long-term stability of the OER, as it is an essential parameter for electrocatalysts. At 50 mA cm⁻², the activity of Ni₂Mo₃N/NF was generally maintained for 5 h with a marginal overpotential increase, shown in Figure 3d. Therefore, the Ni₂Mo₃N/NF catalyst has excellent electrochemical activity and durability for the OER.

Further characterizations, including XRD, XPS, SEM, and TEM measurements, were conducted to monitor the structural changes of Ni₂Mo₃N/NF after the durability test. Figure 4a shows the XRD patterns of the Ni₂Mo₃N/NF catalyst after the 5 h durability test. The Ni₂Mo₃N peaks disappeared, and only metallic Ni peaks were observed, suggesting the transformation of crystalline Ni₂Mo₃N into an amorphous phase during the durability test. In the Ni 2p spectra of Ni₂Mo₃N/NF (Figure 4b), Ni⁰ peaks disappeared, and Ni²⁺ and Ni³⁺ peaks intensified, possibly due to the formation of NiO_x or NiOOH species. The peaks can be deconvoluted into three pairs with binding energies of 855.2/872.5, 856.4/874.2, and 861.3/879.4 eV corresponding to the 2p_{3/2}/2p_{1/2} doublets of Ni²⁺, Ni³⁺, and satellites [27,44,45,51]. In Ni-containing catalysts, surface NiO_x species are generated in

a low potential range below 1.35 V, which are further oxidized to NiOOH at ca. 1.4 V [52,53]. These NiO_x and NiOOH phases are indicated as a significant contributor to the OER performance [27,54]. The Mo 3d XPS spectra in Figure 4c show two pairs with binding energies of 231.7/234.9 and 233.5/235.9 eV, originating from Mo⁵⁺ and Mo⁶⁺ [43,55,56]. Additionally, the intensity of the N 1s spectra was significantly decreased after the durability test (Figure 4d). These results indicate the formation of amorphous surface oxide species from crystalline nitride species. However, in the Ar-sputtered Mo 3d and N 1s spectra of Ni₂Mo₃N/NF after the durability test (Figure S5), the nitride-related peaks appeared again [44,51]. In Figure S1a, Mo⁰ and Mo³⁺ peaks showed up as in the fresh Ni₂Mo₃N/NF sample, and the Mo 3d spectra showed four Mo oxidation states: Mo⁰ (228.3/231.9 eV), Mo³⁺ (229.5/232.6 eV), Mo⁵⁺ (232.0/235.0), and Mo⁶⁺ (233.5/235.8 eV) [43,44,55,56]. In Figure S1b, the intensity of the N 1s spectra increased where metal-N, N-H, and Mo 3p peaks were observed at 397.8, 399.5, and 394.8 eV, respectively [28,31]. These results lead us to conclude that the amorphous surface oxide species were formed after the OER tests, and the metal nitride species remained in the bulk.

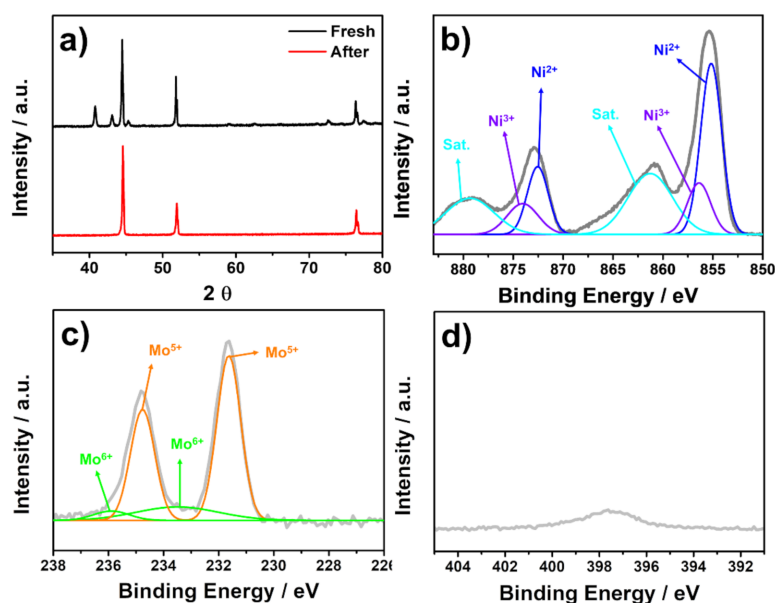


Figure 4. (a) XRD patterns of Ni₂Mo₃N/NF (fresh and after the durability test). XPS spectra of Ni₂Mo₃N/NF after the durability test. (b) Ni 2p, (c) Mo 3d, and (d) N 1s.

SEM and TEM measurements were conducted to inspect the morphologies of the Ni₂Mo₃N/NF after the durability tests (Figure 5). The SEM image in Figure 5a shows that Ni₂Mo₃N remains on the Ni foam similar to fresh Ni₂Mo₃N/NF. SEM-EDS elemental mapping images indicate that the Ni, Mo, and N elements are still uniformly distributed over the Ni foam with a clear O presence due to the formation of amorphous surface oxide species. Nanoparticles less than 10 nm can be observed in the TEM images (Figure 5c,d) without noticeable aggregation. Additionally, the lattice structure of the particles was not observed, indicating the conversion of crystalline Ni₂Mo₃N/NF into amorphous phases.

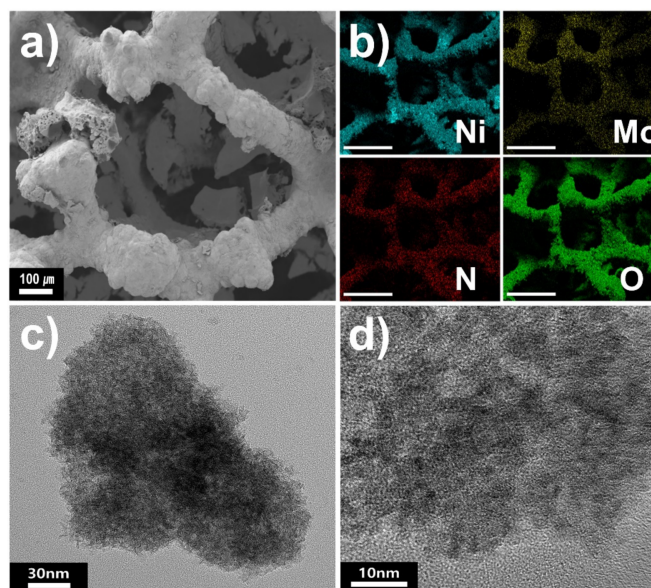


Figure 5. $\text{Ni}_2\text{Mo}_3\text{N}/\text{NF}$ characterization results after the durability tests: (a) SEM images; (b) SEM-EDS elemental mapping images (scale bar = 300 μm); (c,d) TEM images.

4. Conclusions

We prepared $\text{Ni}_2\text{Mo}_3\text{N}$ nanoparticles directly grown on Ni foam using one step, by annealing Ni foam, MoCl_5 , and urea in one pot. The resultant $\text{Ni}_2\text{Mo}_3\text{N}/\text{NF}$ shows impressive electrocatalytic performance for OER in an Fe-purified alkaline electrolyte, with small overpotential values of 336.38 (η_{50}) and 392.49 mV (η_{100}) and good durability for 5 h. The OER tests revealed that the surface of $\text{Ni}_2\text{Mo}_3\text{N}$ converted to amorphous surface oxide species, which might be responsible for its exceptional catalytic activity. Our work offers a facile and economical route for bimetallic nitrides and provides a new avenue for designing highly efficient electrocatalysts.

Supplementary Materials: The following are available online at <https://www.mdpi.com/article/10.3390/ma14164768/s1>, Figure S1: Digital photographs for the synthetic procedure. Figure S2: XRD patterns of prepared samples with various annealing temperatures. Figure S3: Histogram showing the particle size distribution of $\text{Ni}_2\text{Mo}_3\text{N}$ nanoparticles from the TEM images. Figure S4: Cyclic voltammograms of (a) $\text{Ni}_2\text{Mo}_3\text{N}/\text{NF}$, (b) pristine Ni foam and (c) IrO_2 at different scan rates in 1.0 M KOH solution. (d–f) The corresponding current density versus scan rate plots showing C_{dl} values for $\text{Ni}_2\text{Mo}_3\text{N}/\text{NF}$, pristine Ni foam and IrO_2 . Figure S5: XPS spectra of $\text{Ni}_2\text{Mo}_3\text{N}/\text{NF}$ after Ar-sputtering in the (a) Mo 3d and (b) N 1s, respectively. Table S1: Comparison of OER performances in alkaline media with reported TMN-based catalysts.

Author Contributions: Conceptualization, investigation, and writing—original draft, S.H.P.; conceptualization, writing—original draft, and editing, D.H.Y. and S.H.K.; funding acquisition and supervision, D.H.Y. All authors have read and agreed to the published version of the manuscript.

Funding: This research was supported by the R&D Program for Forest Science Technology (FTIS2020 216B10-2022-AC01) provided by the Korea Forest Service (Korea Forestry Promotion Institute) and the National Research Foundation of Korea (NRF) grant funded by the Korea government (Ministry of Education) (2019R1I1A3A01052741). The central laboratory of Kangwon National University and Korea Basic Science Institute (Chuncheon) provided significant assistance with TEM analyses.

Institutional Review Board Statement: Not applicable.

Informed Consent Statement: Not applicable.

Data Availability Statement: The data presented in this study are available upon request from the corresponding author.

Conflicts of Interest: The authors declare no conflict of interest.

References

1. Turner, J.A. Sustainable hydrogen production. *Science* **2004**, *305*, 972–974. [[CrossRef](#)]
2. Ursua, A.; Gandia, L.M.; Sanchis, P. Hydrogen production from water electrolysis: Current status and future trends. *Proc. IEEE* **2012**, *100*, 410–426. [[CrossRef](#)]
3. Lee, G.H.; Lee, M.H.; Kim, Y.; Lim, H.-K.; Youn, D.H. Facile synthesis of nanostructured molybdenum carbide/nitrogen-doped CNT-RGO composite via a modified urea glass route for efficient hydrogen evolution. *J. Alloys Compd.* **2019**, *805*, 113–119. [[CrossRef](#)]
4. Jo, H.M.; Kim, Y.; Youn, D.H. One-pot synthesis of molybdenum carbide/N-doped carbon nanotube composite using nitrilotriacetic acid for efficient hydrogen evolution. *J. Alloys Compd.* **2021**, *855*, 157420. [[CrossRef](#)]
5. Roger, I.; Shipman, M.A.; Symes, M.D. Earth-abundant catalysts for electrochemical and photoelectrochemical water splitting. *Nat. Rev. Chem.* **2017**, *1*, 1–13. [[CrossRef](#)]
6. Girishkumar, G.; McCloskey, B.; Luntz, A.C.; Swanson, S.; Wilcke, W. Lithium–air battery: Promise and challenges. *J. Phys. Chem. Lett.* **2010**, *1*, 2193–2203. [[CrossRef](#)]
7. Xue, Z.; Liu, K.; Liu, Q.; Li, Y.; Li, M.; Su, C.-Y.; Ogiwara, N.; Kobayashi, H.; Kitagawa, H.; Liu, M.; et al. Missing-linker metal-organic frameworks for oxygen evolution reaction. *Nat. Commun.* **2019**, *10*, 1–8. [[CrossRef](#)]
8. Kim, J.-H.; Youn, D.H.; Kawashima, K.; Lin, J.; Lim, H.; Mullins, C.B. An active nanoporous Ni(Fe) OER electrocatalyst via selective dissolution of Cd in alkaline media. *Appl. Catal. B* **2018**, *225*, 1–7. [[CrossRef](#)]
9. Rossmesl, J.; Logadottir, A.; Nørskov, J.K. Electrolysis of water on (oxidized) metal surfaces. *Chem. Phys.* **2005**, *319*, 178–184. [[CrossRef](#)]
10. Reier, T.; Oezaslan, M.; Strasser, P. Electrocatalytic oxygen evolution reaction (OER) on Ru, Ir, and Pt catalysts: A comparative study of nanoparticles and bulk materials. *ACS Catal.* **2012**, *2*, 1765–1772. [[CrossRef](#)]
11. Lyu, F.; Wang, Q.; Choi, S.M.; Yin, Y. Noble-metal-free electrocatalysts for oxygen evolution. *Small* **2019**, *15*, 1804201. [[CrossRef](#)] [[PubMed](#)]
12. Youn, D.H.; Park, Y.B.; Kim, J.Y.; Magesh, G.; Jang, Y.J.; Lee, J.S. One-pot synthesis of NiFe layered double hydroxide/reduced graphene oxide composite as an efficient electrocatalyst for electrochemical and photoelectrochemical water oxidation. *J. Power Sour.* **2015**, *294*, 437–443. [[CrossRef](#)]
13. Fruehwald, H.M.; Moghaddam, R.B.; Melino, P.D.; Ebralidze, I.I.; Zenkina, O.V.; Easton, E.B. Ni on graphene oxide: A highly active and stable alkaline oxygen evolution catalyst. *Catal. Sci. Technol.* **2021**, *11*, 4026–4033. [[CrossRef](#)]
14. Ji, S.; Chen, W.; Zhao, Z.; Yu, X.; Park, H.S. Molybdenum oxynitride nanoparticles on nitrogen-doped CNT architectures for the oxygen evolution reaction. *Nanoscale Adv.* **2020**, *2*, 5659–5665. [[CrossRef](#)]
15. Li, B.; Song, F.; Qian, Y.; Shaw, J.; Rao, Y. Boron-doped graphene oxide-supported nickel nitride nanoparticles for electrocatalytic oxygen evolution in alkaline electrolytes. *ACS Appl. Nano Mater.* **2020**, *3*, 9924–9930. [[CrossRef](#)]
16. Chen, P.; Xu, K.; Tong, Y.; Li, X.; Tao, S.; Fang, Z.; Chu, W.; Wu, X.; Wu, C. Cobalt nitrides as a class of metallic electrocatalysts for the oxygen evolution reaction. *Inorg. Chem. Front.* **2016**, *3*, 236–242. [[CrossRef](#)]
17. Defilippi, C.; Shinde, D.V.; Dang, Z.; Manna, L.; Hardacre, C.; Greer, A.J.; D’Agostino, C.; Giordano, C. HfN nanoparticles: An unexplored catalyst for the electrocatalytic oxygen evolution reaction. *Angew. Chem. Int. Ed.* **2019**, *58*, 15464–15470. [[CrossRef](#)]
18. Walter, C.; Menezes, P.W.; Orthmann, S.; Schuch, J.; Connor, P.; Kaiser, B.; Lerch, M.; Driess, M. A molecular approach to manganese nitride acting as a high performance electrocatalyst in the oxygen evolution reaction. *Angew. Chem.* **2018**, *130*, 706–710. [[CrossRef](#)]
19. Ham, D.; Lee, J. Transition metal carbides and nitrides as electrode materials for low temperature fuel cells. *Energies* **2009**, *2*, 873–899. [[CrossRef](#)]
20. Ningthoujam, R.S.; Gajbhiye, N.S. Synthesis, electron transport properties of transition metal nitrides and applications. *Prog. Mater. Sci.* **2015**, *70*, 50–154. [[CrossRef](#)]
21. Youn, D.H.; Bae, G.; Han, S.; Kim, J.Y.; Jang, J.-W.; Park, H.; Choi, S.H.; Lee, J.S. A highly efficient transition metal nitride-based electrocatalyst for oxygen reduction reaction: TiN on a CNT-graphene hybrid support. *J. Mater. Chem. A* **2013**, *1*, 8007. [[CrossRef](#)]
22. Seol, M.; Youn, D.H.; Kim, J.Y.; Jang, J.-W.; Choi, M.; Lee, J.S.; Yong, K. Mo-compound/CNT-graphene composites as efficient catalytic electrodes for quantum-dot-sensitized solar cells. *Adv. Energy Mater.* **2014**, *4*, 1300775. [[CrossRef](#)]
23. Chen, Q.; Wang, R.; Yu, M.; Zeng, Y.; Lu, F.; Kuang, X.; Lu, X. Bifunctional iron–nickel nitride nanoparticles as flexible and robust electrode for overall water splitting. *Electrochim. Acta* **2017**, *247*, 666–673. [[CrossRef](#)]
24. Liu, X.; Lv, X.; Wang, P.; Zhang, Q.; Huang, B.; Wang, Z.; Liu, Y.; Zheng, Z.; Dai, Y. Improving the HER activity of Ni₃FeN to convert the superior OER electrocatalyst to an efficient bifunctional electrocatalyst for overall water splitting by doping with molybdenum. *Electrochim. Acta* **2020**, *333*, 135488. [[CrossRef](#)]
25. Sankar, M.; Dimitratos, N.; Miedziak, P.J.; Wells, P.P.; Kiely, C.J.; Hutchings, G.J. Designing bimetallic catalysts for a green and sustainable future. *Chem. Soc. Rev.* **2012**, *41*, 8099–8139. [[CrossRef](#)]
26. De, S.; Zhang, J.; Luque, R.; Yan, N. Ni-based bimetallic heterogeneous catalysts for energy and environmental applications. *Energy Environ. Sci.* **2016**, *9*, 3314–3347. [[CrossRef](#)]
27. Yin, Z.; Sun, Y.; Zhu, C.; Li, C.; Zhang, X.; Chen, Y. Bimetallic Ni–Mo nitride nanotubes as highly active and stable bifunctional electrocatalysts for full water splitting. *J. Mater. Chem. A* **2017**, *5*, 13648–13658. [[CrossRef](#)]

28. Zhou, P.; Lv, X.; Xing, D.; Ma, F.; Liu, Y.; Wang, Z.; Wang, P.; Zheng, Z.; Dai, Y.; Huang, B. High-efficient electrocatalytic overall water splitting over vanadium doped hexagonal $\text{Ni}_{0.2}\text{Mo}_{0.8}\text{N}$. *Appl. Catal. B* **2020**, *263*, 118330. [[CrossRef](#)]
29. Yu, L.; Zhu, Q.; Song, S.; McElhenny, B.; Wang, D.; Wu, C.; Qin, Z.; Bao, J.; Yu, Y.; Chen, S.; et al. Non-noble metal-nitride based electrocatalysts for high-performance alkaline seawater electrolysis. *Nat. Commun.* **2019**, *10*, 5106. [[CrossRef](#)]
30. Jia, J.; Zhai, M.; Lv, J.; Zhao, B.; Du, H.; Zhu, J. Nickel molybdenum nitride nanorods grown on Ni foam as efficient and stable bifunctional electrocatalysts for overall water splitting. *ACS Appl. Mater. Interfaces* **2018**, *10*, 30400–30408. [[CrossRef](#)]
31. Chang, B.; Yang, J.; Shao, Y.; Zhang, L.; Fan, W.; Huang, B.; Wu, Y.; Hao, X. Bimetallic NiMoN nanowires with a preferential reactive facet: An ultraefficient bifunctional electrocatalyst for overall water splitting. *ChemSusChem* **2018**, *11*, 3198–3207. [[CrossRef](#)]
32. Trotochaud, L.; Young, S.L.; Ranney, J.K.; Boettcher, S.W. Nickel-iron oxyhydroxide oxygen-evolution electrocatalysts: The role of intentional and incidental iron incorporation. *J. Am. Chem. Soc.* **2014**, *136*, 6744–6753. [[CrossRef](#)]
33. Park, S.H.; Jo, T.H.; Lee, M.H.; Kawashima, K.; Mullins, C.B.; Lim, H.-K.; Youn, D.H. Highly active and stable nickel-molybdenum nitride ($\text{Ni}_2\text{Mo}_3\text{N}$) electrocatalyst for hydrogen evolution. *J. Mater. Chem. A* **2021**, *9*, 4945–4951. [[CrossRef](#)]
34. Youn, D.H.; Han, S.; Kim, J.Y.; Kim, J.Y.; Park, H.; Choi, S.H.; Lee, J.S. Highly active and stable hydrogen evolution electrocatalysts based on molybdenum compounds on carbon nanotube-graphene hybrid support. *ACS Nano* **2014**, *8*, 5164–5173. [[CrossRef](#)] [[PubMed](#)]
35. Giordano, C.; Erpen, C.; Yao, W.; Antonietti, M. Synthesis of Mo and W carbide and nitride nanoparticles via a simple “urea glass” route. *Nano Lett.* **2008**, *8*, 4659–4663. [[CrossRef](#)] [[PubMed](#)]
36. Giordano, C.; Erpen, C.; Yao, W.; Milke, B.; Antonietti, M. Metal nitride and metal carbide nanoparticles by a soft urea pathway. *Chem. Mater.* **2009**, *21*, 5136–5144. [[CrossRef](#)]
37. Michailidis, N.; Stergioudi, F.; Omar, H.; Missirlis, D.; Vlahostergios, Z.; Tsiapas, S.; Albanakis, C.; Granier, B. Flow, thermal and structural application of Ni-foam as volumetric solar receiver. *Sol. Energy Mater. Sol. Cells* **2013**, *109*, 185–191. [[CrossRef](#)]
38. Shah, S.A.; Shen, X.; Yuan, A.; Ji, Z.; Yue, X.; Zhu, G.; Zhou, H.; Xu, K.; Zhu, J.; Chen, Y. One step in-situ synthesis of $\text{Ni}_3\text{S}_2/\text{Fe}_2\text{O}_3/\text{N}$ -doped carbon composites on Ni foam as an efficient electrocatalyst for overall water splitting. *Appl. Surf. Sci.* **2020**, *527*, 146918. [[CrossRef](#)]
39. Zhao, Y.; Jin, B.; Vasileff, A.; Jiao, Y.; Qiao, S.-Z. Interfacial nickel nitride/sulfide as a bifunctional electrode for highly efficient overall water/seawater electrolysis. *J. Mater. Chem. A* **2019**, *7*, 8117–8121. [[CrossRef](#)]
40. Liu, S.; Jiang, Y.; Yang, M.; Zhang, M.; Guo, Q.; Shen, W.; He, R.; Li, M. Highly conductive and metallic cobalt-nickel selenide nanorods supported on Ni foam as an efficient electrocatalyst for alkaline water splitting. *Nanoscale* **2019**, *11*, 7959–7966. [[CrossRef](#)]
41. Herle, P.S.; Hegde, M.; Sooryanarayana, K.; Guru Row, T.; Subbanna, G. $\text{Ni}_2\text{Mo}_3\text{N}$: A new ternary interstitial nitride with a filled β -manganese structure. *Inorg. Chem.* **1998**, *37*, 4128–4130. [[CrossRef](#)]
42. Weil, K.; Kumta, P.; Grins, J. Revisiting a rare intermetallic ternary nitride, $\text{Ni}_2\text{Mo}_3\text{N}$: Crystal structure and property measurements. *J. Solid State Chem.* **1999**, *146*, 22–35. [[CrossRef](#)]
43. Hou, M.; Lan, R.; Hu, Z.; Chen, Z. The preparation of Ni/Mo-based ternary electrocatalysts by the self-propagating initiated nitridation reaction and their application for efficient hydrogen production. *Nanoscale* **2019**, *11*, 17093–17103. [[CrossRef](#)]
44. Yuan, Y.; Adimi, S.; Guo, X.; Thomas, T.; Zhu, Y.; Guo, H.; Priyanga, G.S.; Yoo, P.; Wang, J.; Chen, J.; et al. Surface oxide-rich activation layer (SOAL) on $\text{Ni}_2\text{Mo}_3\text{N}$ for rapid and durable oxygen evolution reaction. *Angew. Chem. Int. Ed.* **2020**, *59*, 18036–18041. [[CrossRef](#)]
45. Zhou, P.; Lv, X.; Gao, Y.; Liang, Z.; Liu, Y.; Wang, Z.; Wang, P.; Zheng, Z.; Dai, Y.; Huang, B. Synthesis of novel cubic $\text{Ni}_2\text{Mo}_3\text{N}$ and its electronic structure regulation by vanadium doping towards high-efficient HER electrocatalyst. *Electrochim. Acta* **2020**, *337*, 135689. [[CrossRef](#)]
46. Zhang, Y.; Ouyang, B.; Xu, J.; Chen, S.; Rawat, R.S.; Fan, H.J. 3D porous hierarchical nickel-molybdenum nitrides synthesized by RF plasma as highly active and stable hydrogen-evolution-reaction electrocatalysts. *Adv. Energy Mater.* **2016**, *6*, 1600221. [[CrossRef](#)]
47. Gong, Y.; Wang, L.; Xiong, H.; Shao, M.; Xu, L.; Xie, A.; Zhuang, S.; Tang, Y.; Yang, X.; Chen, Y.; et al. 3D self-supported Ni nanoparticle@N-doped carbon nanotubes anchored on NiMoN pillars for the hydrogen evolution reaction with high activity and anti-oxidation ability. *J. Mater. Chem. A* **2019**, *7*, 13671–13678. [[CrossRef](#)]
48. Cao, B.; Veith, G.M.; Neuefeind, J.C.; Adzic, R.R.; Khalifah, P.G. Mixed close-packed cobalt molybdenum nitrides as non-noble metal electrocatalysts for the hydrogen evolution reaction. *J. Am. Chem. Soc.* **2013**, *135*, 19186–19192. [[CrossRef](#)] [[PubMed](#)]
49. Li, Y.; Wei, X.; Chen, L.; Shi, J.; He, M. Nickel-molybdenum nitride nanoplate electrocatalysts for concurrent electrolytic hydrogen and formate productions. *Nat. Commun.* **2019**, *10*, 1–12. [[CrossRef](#)]
50. Gong, M.; Li, Y.; Wang, H.; Liang, Y.; Wu, J.Z.; Zhou, J.; Wang, J.; Regier, T.; Wei, F.; Dai, H. An advanced Ni-Fe layered double hydroxide electrocatalyst for water oxidation. *J. Am. Chem. Soc.* **2013**, *135*, 8452–8455. [[CrossRef](#)] [[PubMed](#)]
51. Kawashima, K.; Márquez-Montes, R.A.; Li, H.; Shin, K.; Cao, C.L.; Vo, K.M.; Son, Y.J.; Wygant, B.R.; Chunangad, A.; Youn, D.H.; et al. Electrochemical behavior of a Ni_3N OER precatalyst in Fe-purified alkaline media: The impact of self-oxidation and Fe incorporation. *Mater. Adv.* **2021**, *2*, 2299–2309. [[CrossRef](#)]
52. Shalom, M.; Ressnig, D.; Yang, X.; Clavel, G.; Fellingner, T.P.; Antonietti, M. Nickel nitride as an efficient electrocatalyst for water splitting. *J. Mater. Chem. A* **2015**, *3*, 8171–8177. [[CrossRef](#)]

-
53. Ouyang, B.; Zhang, Y.; Zhang, Z.; Fan, H.J.; Rawat, R.S. Nitrogen-plasma-activated hierarchical nickel nitride nanocorals for energy applications. *Small* **2017**, *13*, 1604265. [[CrossRef](#)] [[PubMed](#)]
 54. Xu, K.; Chen, P.; Li, X.; Tong, Y.; Ding, H.; Wu, X.; Chu, W.; Peng, Z.; Wu, C.; Xie, Y. Metallic nickel nitride nanosheets realizing enhanced electrochemical water oxidation. *J. Am. Chem. Soc.* **2015**, *137*, 4119–4125. [[CrossRef](#)] [[PubMed](#)]
 55. Borgschulte, A.; Sambalova, O.; Delmelle, R.; Jenatsch, S.; Hany, R.; Nuesch, F. Hydrogen reduction of molybdenum oxide at room temperature. *Sci. Rep.* **2017**, *7*, 40761. [[CrossRef](#)]
 56. Tariq, M.; Zaman, W.Q.; Sun, W.; Zhou, Z.; Wu, Y.; Cao, L.-M.; Yang, J. Unraveling the beneficial electrochemistry of IrO₂/MoO₃ hybrid as a highly stable and efficient oxygen evolution reaction catalyst. *ACS Sustain. Chem. Eng.* **2018**, *6*, 4854–4862. [[CrossRef](#)]